Simply synthesized TiO_2 nanorods as an effective scattering layer for quantum dot sensitized solar cells

Mahmoud Samadpour[a)†], Azam Iraji zad[b)c)‡], and Mehdi Molaei[d)]

[a)] *Department of Physics, Faculty of Science, K. N. Toosi University of Technology, P. O. Box* 15418-49611, *Tehran, Iran*
[b)] *Institute for Nanoscience and Nanotechnology, Sharif University of Technology, P. O. Box* 11155-8639, *Tehran, Iran*
[c)] *Department of Physics, Sharif University of Technology, P. O. Box* 11155-9161, *Tehran, Iran*
[d)] *Department of Physics, Faculty of Science,Vali-e-Asr University, Rafsanjan, Iran*

(Received 29 July 2013; revised manuscript received 2 September 2013; published online 10 February 2014)

TiO_2 nanorod layers are synthesized by simple chemical oxidation of Ti substrates. Diffuse reflectance spectroscopy measurements show effective light scattering properties originating from nanorods with length scales on the order of one micron. The films are sensitized with CdSe quantum dots (QDs) by successive ionic layer adsorption and reaction (SILAR) and integrated as a photoanode in quantum dot sensitized solar cells (QDSCs). Incorporating nanorods in photoanode structures provided 4- to 8-fold enhancement in light scattering, which leads to a high power conversion efficiency, 3.03% ($V_{oc} = 497$ mV, $J_{sc} = 11.32$ mA/cm^2, $FF = 0.54$), in optimized structures. High efficiency can be obtained just by tuning the photoanode structure without further treatments, which will make this system a promising nanostructure for efficient quantum dot sensitized solar cells.

Keywords: solar cell, nanorod, quantum dot, scattering

PACS: 73.50.Pz, 73.50.Gr, 81.07.−b, 82.47.Jk **DOI:** 10.1088/1674-1056/23/4/047302

1. Introduction

Dye-sensitized solar cell (DSC) has been proven to be a reliable concept alternative to current p–n junction photovoltaic devices because the functions of both light absorption and charge carrier transport are separated in this system. In a DSC, incident photons are absorbed by molecular dyes that excite the sensitizer electrons. The excited electrons are injected into a porous matrix of a wide band gap semiconductor (e.g. TiO_2) that transfers the photogenerated electrons to the external circuit. Simultaneously, the oxidized dye is regenerated by electron donation from a redox electrolyte.[1–3]

Besides conventional ruthenium dyes, inorganic semiconductors, as alternative sensitizers to dyes in the same configuration of DSCs in order to prepare quantum QDSCs,[4–10] have recently aroused much research interest. In comparison to dyes, narrow-band gap quantum dots (QDs) offer outstanding properties, such as tunability for light absorption by controlling their sizes and compositions, large intrinsic dipole moments,[7] and high molar extinction coefficients.[11,12] Beside these advantages, recent experimental observation of the multiple exciton generation (MEG) in colloidal QDs has made them more attractive for photovoltaic applications.[13–15] However, despite these advantages, the QDSCs still lag in their efficiency in comparison with the conventional DSCs and thus making an efficient QDSC configuration is still a serious challenge.[7,10]

Recently, various approaches have been investigated in order to improve the QDSCs' efficiencies, including TiO_2 surface treatment,[16] photoanode co-sensitization,[17] surface modification of QDs-like ZnS passivation,[18,19] QD-size effect,[20] and doping QDs.[21] Chemical bath deposition (CBD) and successive ionic layer adsorption and reaction (SILAR) methods[20,22] have been utilized instead of direct adsorption methods to increase the number of QDs deposited on TiO_2 photoanode. Co^{2+}/Co^{3+}, polysulphide (S^{2-}/S_x^{2-}) complexes,[23–25] hydrogel,[26] and ionic liquid electrolytes[27] that were used as redox mediators, which are alternatives to the commonly used iodide/triiodide redox couple (I^-/I_3^-) where the most of QDs are unstable. In comparison with generally used Pt counter electrodes in DSCs, more efficient electrodes like CoS,[28] Cu_2S,[29] PbS,[30] carbon nanotubes, mesocellular carbon foam,[31] mesoporous carbon nanofibers,[32] and Graphene oxide[33] are introduced and integrated in QDSCs. However, in spite of these extensive studies, modification to the photoanode structure of QDSC has rarely been conducted and usually the same configuration of DSC photoanodes is used in QDSC. For example, TiO_2 nanoparticulate porous films have been widely used in DSCs and QDSCs due to high surface areas, which result in high efficiencies.[34,35] The pore sizes of these films are typically less than 20 nm.[36,37] Even though this provides a high surface area for good QD loading, pore blocking by QDs and intense electron trapping at both particle surface and grain boundaries can occur.[38] In addition, the electrolyte permeation will be

†Corresponding author. E-mail: samadpour@kntu.ac.ir
‡Corresponding author. E-mail: iraji@sharif.edu

© 2014 Chinese Physical Society and IOP Publishing Ltd

restricted, leading to poor photovoltaic properties.[39]

Reviewing the literature indicates that noticeable photovoltaic results in QDSCs have mainly been obtained using different photoanode structures rather than convenient TiO_2 nanoparticulate porous structures. A close to 5% efficiency for CdS/CdSe quantum dot sensitized cells was obtained by using precisely designed TiO_2 photoanode structures by the Toyoda group.[34] To the best of our knowledge, the highest open circuit photovoltage in QDSCs has been obtained by using ZnO nanowires and Si/ZnO branched hierarchical structures by Sudhagar *et al.*[40] We have used nanostructured hollow fibers in QDSCs and the cells efficiency was noticeably increased from 0.66% to more than 3% just by controlling the photoanode structure.[41] Recently, we have shown a clear correspondence between photovoltaic conversion efficiency and TiO_2 photoanode structural properties, and have proved that higher V_{oc} values can systematically be obtained in TiO_2 morphologies by reducing the surface area.[42] While effective configuration for working electrodes have been proposed for DSSCs, the optimized photoanode structure for QDSCs is not yet obtained and more research should be done in this regard.

In this paper, we show that efficient QDSCs can be obtained by simply fabricating the TiO_2 photoanode structures. We show that the efficiency can be easily improved by precise monitoring of the optical and electrical properties of the photoanode. In this sense, we introduce here TiO_2 nanorods as effective light scattering structures to make efficient QDSCs by optimizing the photoanode structure. The samples are synthesized by simple chemical oxidation of titanium foil at a moderate temperature of 80 °C. The nanorods have length scales on the order of one micron while their average diameter is about 50 nm. The micron length of the nanorod structures gives rise to interesting light scattering properties, as characterized by diffuse reflectance spectroscopy. On the other hand, electronic transport can be potentially improved in these one-dimensional systems. Besides the above mentioned properties, this structure also prevents the pores from being blocked by QDs and is conducible to the electrolyte diffusing deeply into the photoanode. More than 3% efficiency is obtained, which is higher than 2.34% for conventional QDSCs made by 20-nm-sized nanocrystalline TiO_2 (18 NR-T, Dyesol). We show that the enhanced photovoltaic performance of QDSCs can be obtained by the accurate monitoring of the QD loading, light scattering, and electron recombination in photoanode structure.

2. Experiment

2.1. Synthesis of the nanorods

TiO_2 nanorods were simply synthesized as previously described.[43] In brief, titanium foils were cleaned by sonication in acetone and deionized (DI) water in sequence for 10-min. The samples were then put in a mixture of 10-mL hydrofluoric acid (40%) and 15-mL nitric acid (63%) for 10 s. Finally, the samples were sonicated for 10 min in DI water and dried in nitrogen flow. The cleaned titanium pieces were immersed in 10 mL of 30% W hydrogen peroxide solution and kept at 80 °C for 72 h. The samples were then removed and rinsed with DI water and dried in air. Heat treatment process in oxygen flow was performed by increasing the temperature with a rate of 10 °C/min to 500 °C and maintaining this temperature for 3 h. These nanorods were detached from the Ti substrate and were used to make nanorod based pastes.

2.2. Electrode preparation

Three different TiO_2 pastes were used to prepare the electrodes. The first paste was "18NR-T Dyesol" containing 20-nm TiO_2 nanoparticles, which is used to make high surface area transparent TiO_2 layers; we name this paste "T". For the second paste, 1 g of ethyl cellulose was dissolved in 12.5-mL ethanol assisted by ultrasonication. The paste was prepared by milling 0.2-g TiO_2 nanorods and 1-mL prepared ethyl cellulose in ethanol in a mortar for 30 min while 1-mL terpineol was added drop by drop in the milling process. We name this paste "N". The third paste was 18NR-AO (TiO_2 particle size 20 nm–450 nm) from Dyesol Company, which is commonly employed to create light scattering layers in DSCs and QDSCs. We name this paste "S". Seven different electrode configurations were prepared as photoanodes in QDSCs by using these three TiO_2 pastes.

The photoanodes were doctor-bladed on transparent conducting fluorine-doped tin oxide (FTO) glass substrates (sheet resistance $\sim 10\ \Omega/\square$). The resulting photoelectrodes were sintered at 450 °C to obtain better electrical contact of the nanoparticles and nanoparticles with the substrate. Before doctor-blading, a compact layer of TiO_2 was deposited on FTO substrates by spray pyrolisis ($\sim$ 100-nm thick). These electrodes were calcinated at 450 °C for 30 min.

2.3. Electrode sensitization

TiO_2 electrodes were *in situ* sensitized by CdSe QDs grown by SILAR. The SILAR process was carried out following the method developed in Ref. [44]. In brief, 0.03-M $Cd(NO_3)_2$ in ethanol was used as the Cd^{+2} source and the *in situ* prepared 0.03-M Se^{2-} in ethanol was used as an Se^{2-} precursor. For sensitization, the electrodes were successively dipped in these solutions inside a glove box under N_2 atmosphere. One SILAR cycle for CdSe consisted of 30-second dipping of the TiO_2 working electrode into the Cd^{2+} precursor and subsequently into the selenide solution for the same length of time. Following each bath, the photoanode was rinsed in pure ethanol to remove the chemical residuals from the surface and then dried with an N_2 gun. In order to improve the stability and performance of the cells, all of the samples were deposited

with a ZnS protective coating,[45,46] by being dipped into 0.1-M $Zn(CH_3COO)_2$ and 0.1-M Na_2S solutions for 1 min twice in sequence, and then by being rinsed with Milli-Q ultrapure water between dips.[46]

2.4. QDSC preparation

The cells were prepared by sandwiching a scotch spacer (thickness 50 μm) between the Cu_2S counter electrode and a QD-sensitized electrode and permeating polysulfide electrolyte. Polysulfide electrolyte was 1-M Na_2S, 1-M S, and 0.1-M NaOH solution in Milli-Q ultrapure water. We used Cu_2S counter electrodes for clamping the sensitized electrode and the counter electrode.[47] The electrodes were prepared by immersing brass in HCl solution at 70 °C for 5 min and subsequently dipping it into polysulfide solution for 10 min, resulting in a porous Cu_2S electrode. The area of the cells was 0.28 cm^2.

2.5. Photoanode and solar cell characterization

The optical absorption spectra of the photoanodes were recorded at 300 nm–800 nm by a Cary 500 UV-VIS Varian spectrometer. The *J*–*V* curves, impedance spectroscopy (IS) measurement, and applied bias voltage decay (ABVD)[48] were carried out with an FRA equipped PGSTAT-30 from Autolab. The *J*–*V* measurements were carried out using a mask (0.24 cm^2) and no antireflective layer was used. Cells were illuminated using a solar simulator at AM1.5 G, where the light intensity was adjusted with an NREL calibrated Si solar cell with a KG-5 filter to one sun intensity (100 mW/cm^2). Incident photon-to-electron conversion efficiency (IPCE) measurements have been performed employing a 150-W Xe lamp coupled with a computer-controlled monochromator, the photocurrent was measured using a nanoamperimeter 70310 from Oriel Instruments. Impedance spectroscopy measurements were carried out in dark conditions by applying a 20-mV AC signal in a frequency range between 400 kHz and 0.1 Hz at various forward biases.

3. Results and discussion

Representative SEM micrographs of the nanorods (N), T, and S structures are shown in Figs. 1(a)–1(c). The average diameter of the rods is around 50 nm (Fig. 1(c)); consequently, a moderate-high surface area of the nanorods is expected for QDs sensitization. XRD patterns (see Fig. S1 in Appendix A) reveal that the synthesized nanorods have anatase crystalline structures.

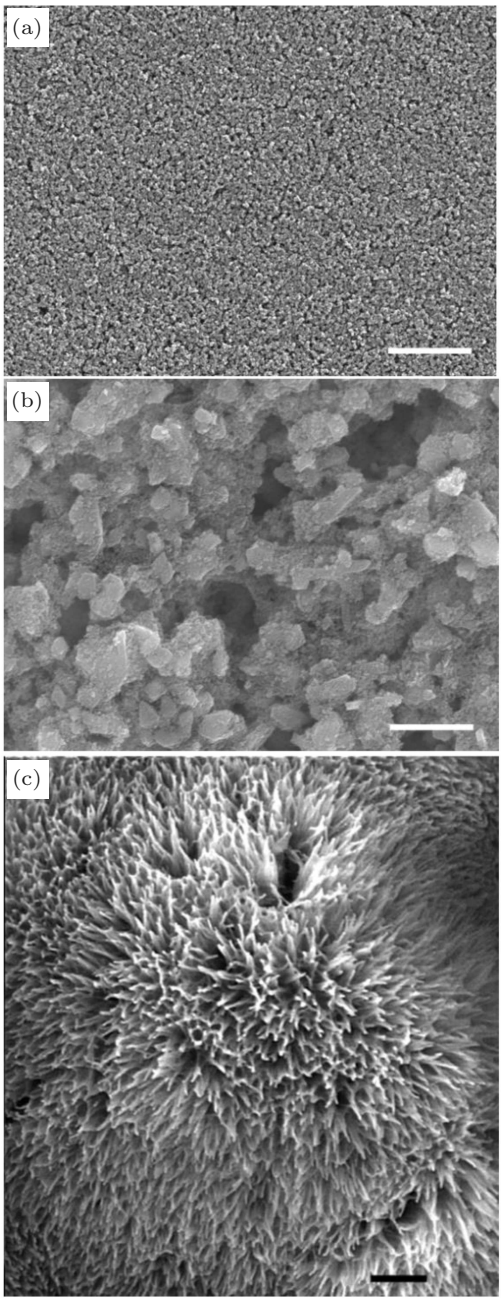


Fig. 1. SEM micrographs from T (a), S (b), and N (c) structures. Scale bar is 1 μm for panels (a), (b), and (c).

Considering the scattering properties originating from micron length and the moderate-high surface area of these nanorods, various structures of TiO_2 photoanodes are designed in order to find the most efficient cells. Three kinds of pastes: T (TiO_2 paste with 20-nm nanoparticles), N (paste with TiO_2 nanorods), and S (paste with 20 nm–450 nm TiO_2 nanoparticles) are used to prepare the different photoanode structures (see experimental section for more details). The 1, 2 or 3 layers of TiO_2 paste are doctor bladed on the FTO substrates. We label the structures as "ABC": A, B, and C, referring to the type of the paste (T, N or S) which is used for the first, second, and third layers on the FTO substrate, respectively. For example, the TNN structure means that we have deposited three

layers of TiO_2 on FTO, the first layer is prepared with T-type paste and the second and third layers are prepared with N-type paste. Seven different structures are tested as photoanodes, as shown in Fig. 2. The TT structure (the only structure without nanorods) is prepared as a reference to compare its light scattering properties with those of other photoanodes.

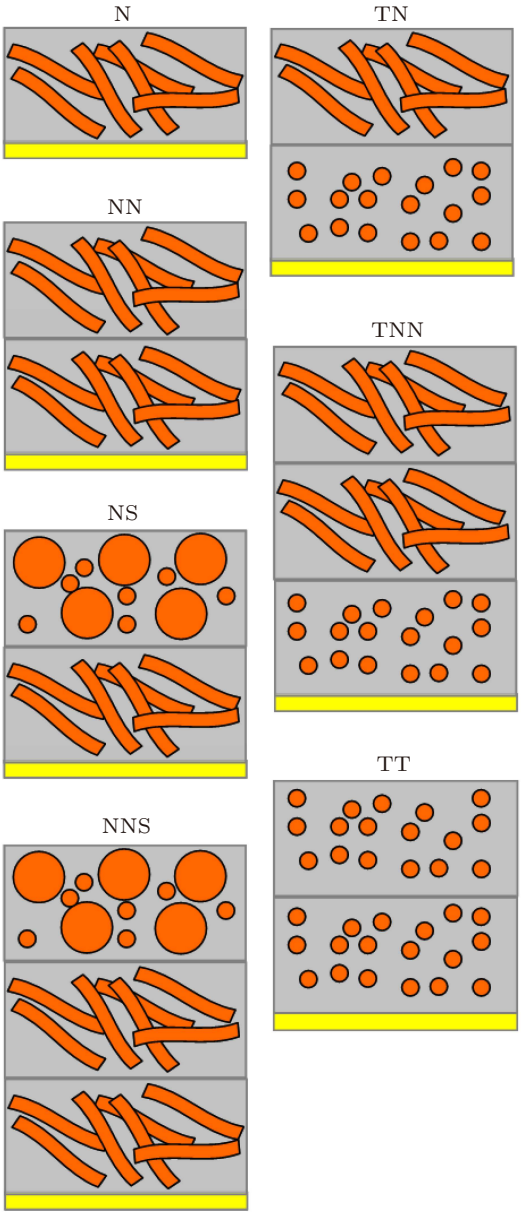


Fig. 2. (color online) Schematics of the seven photoanode structures (N, NN, NS, NNS, TN, TNN, TT) in QDSCs: T layer that has 20-nm TiO_2 nanoparticles, a high surface area for sufficient QDs adsorption, small pores that could be blocked during QDs deposition and thus prevent electrolyte diffusion, and non-direct path for electron transport; N layer that has photoanode based on TiO_2 nanorods, low surface area compared with nanoparticulated anode, direct path for electron transport, efficient scattering properties; S layer that has 20 nm–450 nm TiO_2 nanoparticles, smaller particles that make high surface area for sufficient QD adsorption, larger particles acting as scattering particles, non-direct path for electron transport. The thickness of N structure is (5 ± 1) μm, and the thickness values of T and S structures are both (6 ± 1) μm.

The light scattering properties of these structures without QD sensitization are measured by diffuse reflectance spectroscopy (see Fig. 3). The TT sample clearly shows the lowest light scattering properties while considerable scattering effect can be seen from the structures containing nanorods. Up to four times scattering enhancement with just one layer of nanorods, N structure, can be inferred from the more intense diffuse reflectance of this sample at longer wavelengths that TiO_2 does not absorb (see Fig. 3). The light scattering properties of layers made by the nanorods are enhanced by four-to-eight fold, depending on structure, compared with those of the TT structures (see Fig. 3).

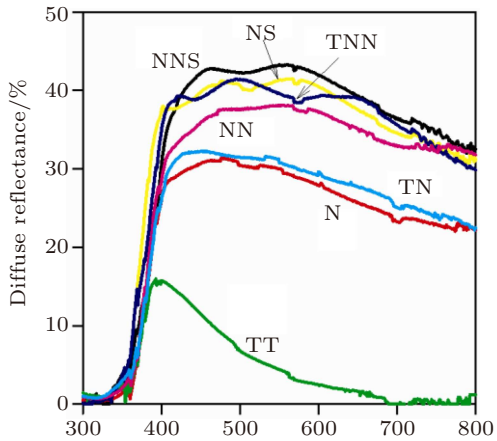


Fig. 3. (color online) Diffuse reflectance spectra of different TiO_2 structures made by T, S, and N pastes.

These seven different structures are sensitized by seven SILAR cycles of CdSe quantum dots and then coated with ZnS, as mentioned in the experimental section. Table 1 shows the solar cell parameters obtained for these QDSCs: photocurrent j_{sc}, open circuit voltage V_{oc}, fill factor FF, and efficiency η, depending on photoanode structures, obtained from the test under a standard condition (100 mW/cm^2 AM 1.5 G).

Table 1. Photovoltaic parameters of the QDSCs prepared: photocurrent j_{sc}, open circuit voltage V_{oc}, fill factor FF, and efficiency η, depending on cell structures sensitized by SILAR, obtained from the test under a standard light illumination condition (100 mW/cm^2 AM 1.5 G).

Cell	V_{oc}/mV	J_{sc}/(mA/cm^2)	FF	η/%
N	520	6.38	0.44	1.46
NN	528	9.49	0.46	2.34
NS	537	11.43	0.46	2.84
NNS	497	6.80	0.52	1.76
TN	497	11.32	0.54	3.03
TNN	488	9.04	0.54	2.38
TT	467	9.75	0.51	2.34

As shown in Table 1, increasing the number of TiO_2 layers give rise to two opposing effects. On one hand, we expect the enhancement in light harvesting due to the larger amount of light absorbing sensitizer because of higher thickness of photoanode. On the other hand, for thicker samples, the effective surface of the electrode concomitantly increases, causing an enhancement of recombination. In this sense, a balance among light scattering, QD loading, and recombination is mandatory

to optimize the QDSC performance. So, in Table 1 the highest efficiencies have been obtained from TN samples, each of which has an intermediate diffuse reflectance (see Fig. 3).

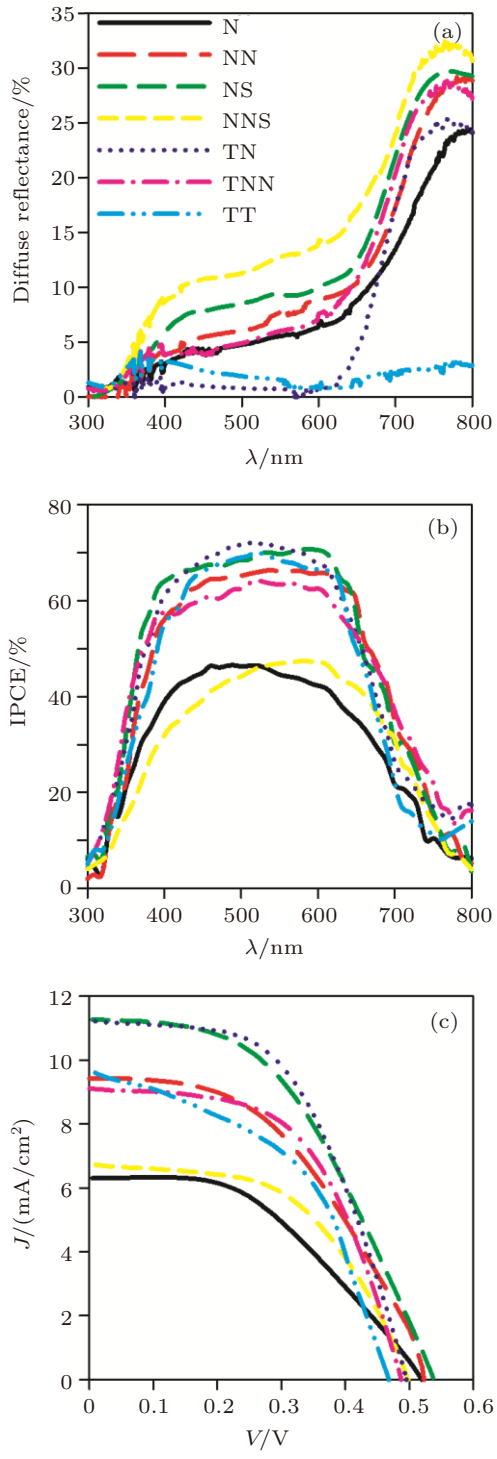


Fig. 4. (color online) (a) Diffuse reflectances, (b) IPCE, and (c) *J*–*V* curves for SILAR sensitized cells.

The best efficiencies are obtained with the TN (3.03%) and NS (2.84%) structures (see Table 1). Representative diffuse reflectance, IPCE, and current–voltage (*J*–*V*) curves obtained for SILAR sensitized cells are plotted in Figs. 4(a)–4(c), respectively. From Fig. 3 it can be seen that TNN and NNS structures indicate the enhanced light scattering properties in comparison with TN and NS structures, respectively. In addition, more QDs are deposited in TNN and NNS structures than in TN and NS structures, respectively. Regarding the enhancement in light scattering and QDs deposition in TNN and NNS structures, it is expected to obtain better photovoltaic efficiencies in these structures than in TN and NS structures.

From Table 1 it can be seen that, inconsistently with our expectations, the good efficiency of the TN (3.03%) and NS structures (2.84%) has decreased to 2.38% and 1.78%, respectively, after depositing one more layer of nanorods on the top of TN structure (TNN structure) and depositing one more N layer in NS structures (NNS). The measured IPCEs for the NN, NS, TN, and TT structures sensitized by SILAR are very similar and the IPCE for the NNS structure is clearly reduced compared with these structures, which is in good agreement with the finally obtained photocurrents as shown in Fig. 4(c).

To better understand the physical characteristics of these solar cells, impedance spectroscopy measurements and ABVD are carried out on QDSCs. Chemical capacitance, C_μ (Fig. 5(a)) and recombination resistance, R_{rec} (Fig. 5(b)) are obtained from IS measurements using the previously developed model.[49,50] The C_μ is plotted against the voltage drop in the sensitized electrode, V_F. This voltage is obtained by subtracting the voltage drop of the series resistance, V_{series}, from applied voltage in the IS measurements, V_{app}, and given by $V_F = V_{app} - V_{series}$. The R_{rec} is plotted against the voltage drop in a common equivalent conduction band (CB), V_{ecb}, where the effect of different TiO_2 CB between samples is removed.[50] Plotting R_{rec} against V_{ecb} allows the analysis of the recombination resistance on the basis of an equal density of electrons n (i.e., the same distance between the electron Fermi level and the TiO_2 conduction band). This procedure is carried out by shifting V_F until the chemical capacitance overlaps (see also Fig. S2 in Appendix A). The methods to obtain the dependences against V_F and V_{ecb} from IS measurements have been previously reported.[50–52]

Considering the chemical capacitance (Fig. 5(a)), all the samples show very similar slopes for C_μ, indicating a similar density of states.[50] On the other hand, C_μ is shifted, indicating a displacement of the TiO_2 CB.

Taking the TN sample as a reference, a downward shift of TiO_2 CB band is observed in the TNN, TT, NS, and NNS samples (Fig. 5(a)). After correcting this shift, the TN and NS samples each show a higher recombination resistance (the lowest recombination) (see Fig. 5(b)). The recombination resistances of TNN and NNS samples decrease in comparison with those of TN and NS structures, respectively. This arises from the larger thickness values of NNS and TNN [(15 ± 1) μm] structures (and consequently larger effective surface)[38] than those of the NS and TN samples [(11 ± 1) μm], respectively.

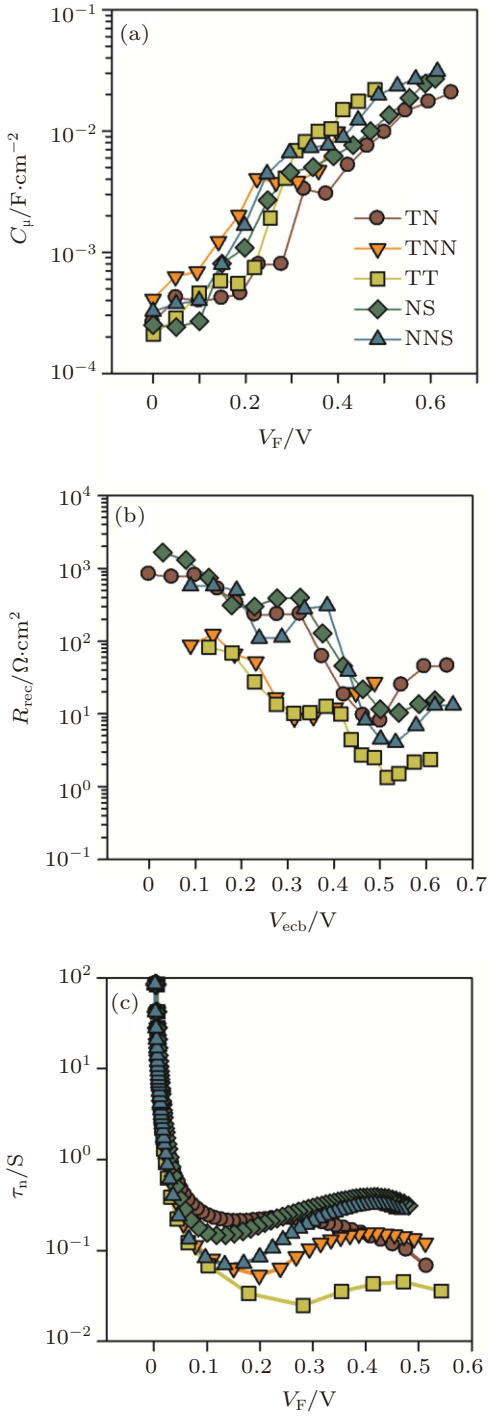


Fig. 5. (color online) (a) Chemical capacitance versus V_F , (b) recombination resistance versus V_{ecb}, and (c) electron lifetime versus V_F for QDSCs. Chemical capacitance and recombination resistance are obtained from IS measurements[50] while electron lifetime is obtained from ABVD measurements.[48]

This reduced recombination resistance is in good agreement with the higher dark currents obtained for these cells (see Fig. S3 in Appendix A). According to Fig. 5(b), the TT sample shows the lowest recombination resistance (consequently higher dark current), which is consistent with the highest dark current in this cell (see Fig. S3 in Appendix A). In addition, the lower recombination resistances of the TT samples are confirmed by comparing the values of electron life time (τ_n) of the samples (Fig. 5(c)). The value of τ_n has been measured by ABVD[46] under dark condition, as measured by IS. Conversely, the highest efficient cells with TN (3.03%) and NS structures (2.84%), see Table 1, have the highest recombination resistances (Fig. 5(b)), which is confirmed by high electron life times in these cells (Fig. 5(c)). This fact points out a remarkable influence of recombination on QDSC performance. The valleys observed in R_{rec} curves, see Fig. 5(b), can be related to recombination through surface states, as discussed elsewhere.[8,53]

4. Conclusions

We have synthesized TiO_2 nanorods by oxidation of Ti foil with a simple chemical method. The unique properties of nanorods (i.e. enough surface area, effective light scattering, and a one-dimensional structure that is conducible to electron transport) give rise to an increase in the efficiency of the QDSC. We sensitize various TiO_2 structures with CdSe QDs that are grown by the SILAR method as photoanodes. High power conversion efficiency ($\eta = 3.03\%$, $V_{oc} = 497$ mV, $J_{sc} = 11.32$ mA/cm^2, $FF = 0.54$) is obtained using a transparent layer (T) and efficient light scattering layer of nanorods (N) in TN structure. The unique properties of these nanorods and the rather high efficiencies obtained here suggest that TiO_2 nanorods are promising materials to develop high efficient QDSCs. It is also highlighted that the photoanode structure plays a determinant role in the final cell performance. A rational balance among QD loading, light scattering, and recombination is mandatory in order to optimize the performance of the photoanode for QDSCs.

Appendix A

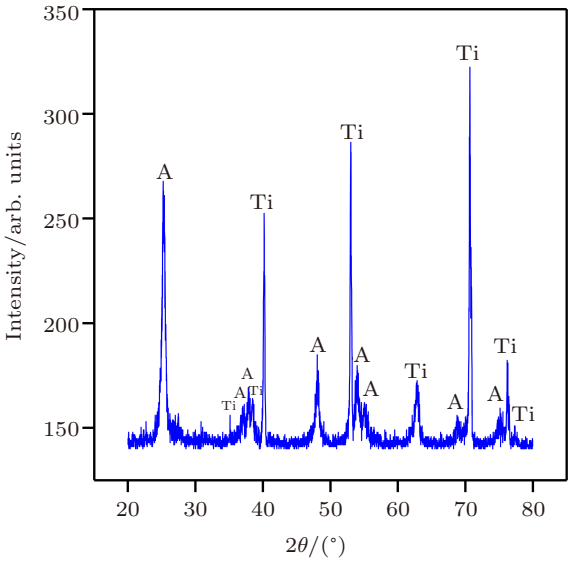


Fig. S1. (color online) XRD patterns of synthesized TiO_2 nanorods on Ti substrate, Ti picks are related to substrate (A: anatase, Ti: titanium).

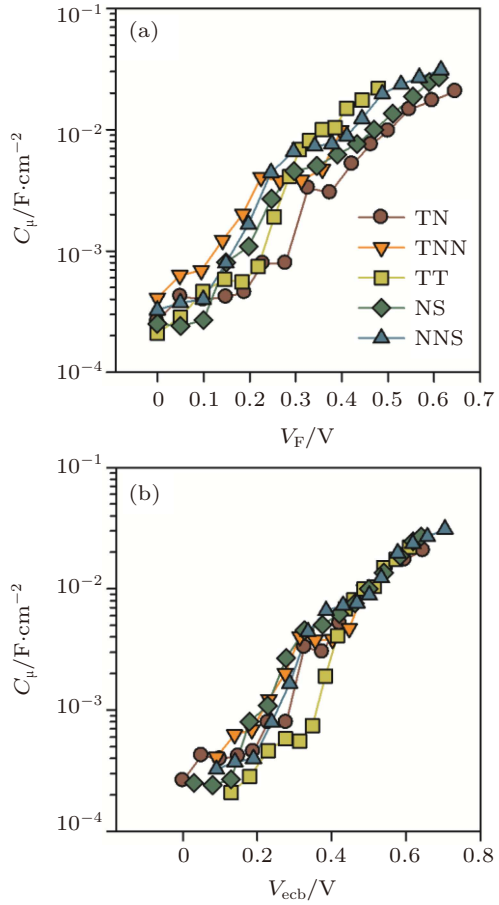


Fig. S2. (color online) Correcting the effect of the position of the TiO_2 conduction band. Voltage shift has been applied to the different C_μ curves plotted in (a) (Fig. 5(a)) to make them overlap in order to correct the effect of TiO_2 conduction band displacement in SILAR sensitized cells. The same shift performed on the chemical capacitance in panel (b) has been carried out on the recombination resistance in order to plot it against V_{ecb}, see Fig. 5(b). Here, sample TN has been taken as a reference sample and voltage shift has been applied to the C_μ curves of TNN, TT, NS, and NNS samples to make them overlap.

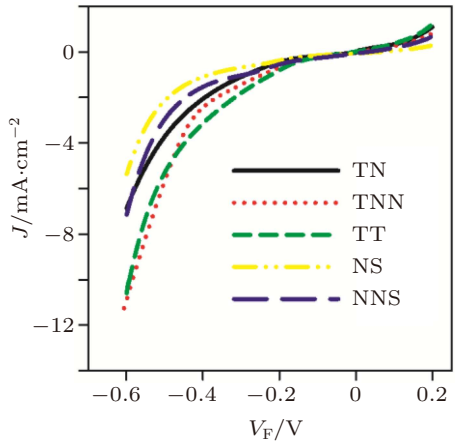


Fig. S3. (color online) Measured dark currents for TN, TNN, TT, NS, and NNS TiO_2 structures.

References

[1] Bisquert J, Cahen D, Hodes G, Rühle S and Zaban A 2004 *J. Phys. Chem. B* **108** 8106

[2] Tao X B, Xue Z B, Jing B, Qing Z, Biao L Y, Min C W and Jun C 2008 *Chin. Phys. B* **17** 3713

[3] Jian L P, Kai C, Fu C Y, Gao W Z, Xin H, Bo L J, Rui H J and Li Z W 2012 *Chin. Phys. B* **21** 118101

[4] Hodes G 2008 *J. Phys. Chem. C* **112** 17778

[5] Kamat P V 2008 *J. Phys. Chem. C* **112** 18737

[6] Kamat P V, Tvrdy K, Baker D R and Radich J G 2010 *Chem. Rev.* **110** 6664

[7] Mora-Seró I and Bisquert J 2010 *J. Phys. Chem. Lett.* **1** 3046

[8] Mora-Seró I, Giménez S, Fabregat-Santiago F, Gómez R, Shen Q, Toyoda T and Bisquert J 2009 *Accounts of Chemical Research* **42** 1848

[9] O'Regan B and Grätzel M 1991 *Nature* **353** 737

[10] Rühle S, Shalom M and Zaban A 2010 *Chem. Phys. Chem.* **11** 2290

[11] Alivisatos A P 1996 *Science* **271** 933

[12] Yu W W, Qu L, Guo W and Peng X 2003 *Chem. Mater.* **15** 2854

[13] Ellingson R J, Beard M C, Johnson J C, Yu P, Micic O I, Nozik A J, Shabaev A and Efros A L 2005 *Nano Lett.* **5** 865

[14] Sambur J B, Novet T and Parkinson B A 2010 *Science* **330** 63

[15] Schaller R D and Klimov V I 2004 *Phys. Rev. Lett.* **92** 186601

[16] Samadpour M, Boix P P, Giménez S, Iraji Zad A, Taghavinia N, Mora-Seró I and Bisquert J 2011 *J. Phys. Chem. C* **115** 14400

[17] Y L Lee and Y S Lo 2009 *Adv. Func. Mater.* **19** 604

[18] Mora-Seró I, Giménez S, Fabregat-Santiago F, Gómez R, Shen Q, Toyoda T and Bisquert J 2009 *Acc. Chem. Res.* **42** 1848

[19] Shen Q, Kobayashi J, Diguna L J and Toyoda T 2008 *J. Appl. Phys.* **103** 084304

[20] Kongkanand A, Tvrdy K, Takechi K, Kuno M and Kamat P V 2008 *J. Am. Chem. Soc.* **130** 4007

[21] Santra P K and Kamat P V 2012 *J. Am. Chem. Soc.* **134** 2508

[22] Robel I, Subramanian V, Kuno M and Kamat P V 2006 *J. Am. Chem. Soc.* **128** 2385

[23] Lee H J, Chen P, Moon S J, Sauvage F, Sivula K, Bessho T, Gamelin D R, Comte P, Zakeeruddin S M, Seok S I, Grätzel M and Nazeeruddin M K 2009 *Langmuir* **25** 7602

[24] Lee Y L and Chang C H 2008 *J. Power Sources* **185** 584

[25] Li L, Yang X, Gao J, Tian H, Zhao J, Hagfeldt A and Sun L 2011 *J. Am. Chem. Soc.* **133** 8458

[26] Yu Z, Zhang Q, Qin D, Luo Y, Li D, Shen Q, Toyoda T and Meng Q 2010 *Electrochem. Commun.* **12** 1776

[27] Jovanovski V, González-Pedro V, Giménez S, Azaceta E, Cabañero G, Grande H, Tena-Zaera R, Mora-Seró I and Bisquert J 2011 *J. Am. Chem. Soc.* **133** 20156

[28] Yang Z, Chen C Y, Liu C W, Li C L and Chang H T 2011 *Adv. Energy Mater.* **1** 259

[29] Deng M, Huang S, Zhang Q, Li D, Luo Y, Shen Q, Toyoda T and Meng Q 2010 *Chem. Lett.* **39** 1168

[30] Tachan Z, Shalom M, Hod I, Rühle S, Tirosh S and Zaban A 2011 *J. Phys. Chem. C* **115** 6162

[31] Seol M, Ramasamy E, Lee J and Yong K 2011 *J. Phys. Chem. C* **115** 22018

[32] Fang B, Kim M, Fan S Q, Kim J H, Wilkinson D P, Ko J and Yu J S 2011 *J. Mater. Chem.* **21** 8742

[33] Santra P K and Kamat P V 2012 *J. Am. Chem. Soc.* **134** 2508

[34] Zhang Q, Guo X, Huang X, Huang S, Li D, Luo Y, Shen Q, Toyoda T and Meng Q 2011 *Phys. Chem. Chem. Phys.* **13** 4659

[35] González-Pedro V, Xu X, Mora-Seró I and Bisquert J 2010 *ACS Nano* **4** 5783

[36] Barbé J C, Arendse F, Comte P, Jirousek M, Lenzmann F, Shklover V and Grätzel M 1997 *J. Am. Ceram. Soc.* **80** 3157

[37] Ito S, Murakami T N, Comte P, Liska P, Grätzel C, Nazeeruddin M K and Grätzel M 2008 *Thin Solid Films* **516** 4613

[38] Guijarro N, Lana-Villarreal T, Shen Q, Toyoda T and Gómez R 2010 *J. Phys. Chem. C* **114** 21928

[39] Sudhagar P, Jung J H, Park S, Lee Y G, Sathyamoorthy R, Kang Y S and Ahn H 2009 *Electrochem. Commun.* **11** 2220

[40] Sudhagar P, Song T, Lee D H, Mora-Seró I, Bisquert J, Laudenslager M, Sigmund W M, Park Won Il, Paik U and Kang Y S 2011 *J. Phys. Chem. Lett.* **2** 1984

[41] Samadpour M, Giménez S, Iraji-Zad A, Taghavinia N and Mora-SeróI 2012 *Phys. Chem. Chem. Phys.* **14** 522

[42] Samadpour M, Giménez S, Boix P P, Shen Q, Calvo M E, Taghavinia N, Iraji-Zad A, Toyoda T, Míguez H and Mora-Seró I 2012 *Electrochimica Acta* **75** 139

[43] Samadpour M, Taghavinia N, Iraji-Zad A, Marandi M and Tajabadi F 2012 *Euro. Phys. J: Appl. Phys.* **57** 20401
[44] Lee H, Wang M, Chen P, Gamelin D R, Zakeeruddin S M, Grätzel M and Nazeeruddin M K 2009 *Nano Lett.* **9** 4221
[45] Lee H J, Bang J, Park J, Kim S and Park S M 2010 *Chem. Mater.* **22** 5636
[46] Shen Q, Kobayashi J, Diguna L J and Toyoda T 2008 *J. Appl. Phys.* **103** 084304
[47] Hodes G, Manassen J and Cahen D 1980 *J. Electrochem. Soc.* **127** 544
[48] Bisquert, J, Zaban A, Greenshtein M and Mora-Seró I 2004 *J. Am. Chem. Soc.* **126** 13550
[49] Fabregat-Santiago F, Bisquert J, Garcia-Belmonte G, Boschloo G and Hagfeldt A 2005 *Solar Energy Materials and Solar Cells* **87** 117
[50] Fabregat-Santiago F, Garcia-Belmonte G, Mora-Seró I and Bisquert J 2011 *Phys. Chem. Chem. Phys.* **13** 9083
[51] Barea E M, Shalom M, Giménez S, Hod I, Mora-Seró I, Zaban A and Bisquert J 2010 *J. Am. Chem. Soc.* **132** 6834
[52] Braga A, Giménez S, Concina I, Vomiero A and Mora-Seró I 2011 *J. Phys. Chem. Lett.* **2** 454
[53] Hod I, González-Pedro V, Tachan Z, Fabregat-Santiago F, Mora-Seró I, Bisquert J and Zaban A 2011 *J. Phys. Chem. Lett.* **2** 3032